Polarimetric Characterization of Ultrawideband Propagation Channels

Wasim Q. Malik, *Member, IEEE*

Abstract—The polarization characteristics of the indoor ultra-wideband channel are investigated using dual-polar 3.1–10.6 GHz channel measurements. Under the generalized elliptical polarization framework, the channel cross-polar discrimination (XPD) statistics are evaluated. Lognormal and triangular distributions are shown to well model the XPD and ellipticity angle. Considerable spectral and small-scale spatial variability is observed in the XPD. Asymptotic convergence of XPD to its mean with increasing bandwidth is established. An analysis of the variation of tap XPD with excess delay indicates that the XPD is highest for the initial paths. It is shown that increased scattering leads to greater depolarization. The dependence of XPD on the channel's rms delay spread is modelled using a linear regression with -0.5 dB/ns slope. This characterization will aid the analysis of polarization-dependent loss and the design of polarized multiple-antenna systems.

Index Terms—Channel characterization, cross-polar discrimination (XPD), polarization, ultrawideband (UWB).

I. INTRODUCTION

DUE TO STRONG frequency-selectivity, the propagation characteristics of ultrawideband (UWB) wireless channels differ considerably from those of conventional narrowband channels [1]. The characterization of various aspects of UWB propagation is a topic of continued interest. A number of UWB channel characterization studies have been undertaken in recent years [1], [2], focussing mostly on the analysis of fading, dispersion and spatial propagation. Another important physical attribute of the channel is its electromagnetic polarization behavior. If the transmitting and receiving antennas are perfectly co-polarized, as is usually desirable, but the channel rotates the signal polarization, the receiver may fail to capture much of the signal power. Such a situation then requires a polar antenna diversity system with multiple effective degrees of freedom [3]–[7]. Similarly, polar multiple-input multiple-output (MIMO) arrays can be used to increase the information rate by signal multiplexing [7]–[11]. With its compact design, a polar array is desirable for many practical applications [12]. The performance prediction of a polar MIMO system requires accurate polarimetric characterization of the channel.

From the perspective of polarization, there are some major shortcomings in the existing UWB channel studies that deserve attention. The transmitted and received signals are usually assumed to be perfectly co-polar. This is unrealistic especially in indoor channels where three-dimensional propagation and multiple reflections are likely to cause significant signal depolarization. Furthermore, the loss due to polarization mismatch is included within the pathloss. This leads to a complete lack of information about signal depolarization loss, erroneously implying perfect polarization preservation by the channel.

The polarization characterization literature mostly addresses narrowband channels [13]–[16]. Mean cross-polar discrimination (XPD) of 6–7 dB has been widely reported for most narrowband mobile environments [3], [17]–[20]. Signal depolarization is an entropic effect that increases with the amount of scattering in the channel [21]. Indoor and non-line-of-sight (NLOS) radio environments, which experience rich multipath, demonstrate lower values of XPD than outdoor, line-of-sight (LOS) channels [18], [22]. The polarization response of an object also generally varies with the signal frequency and angle of incidence. For these reasons, it is reasonable to expect that the results for narrowband outdoor mobile channels cannot be directly applied to UWB indoor channels. To the author's knowledge, no UWB channel polarization model is available in the literature. A preliminary UWB polarization measurement system was introduced in [23] but no results were presented.

The contribution of this paper is the comprehensive statistical characterization of channel polarization in the UWB indoor environment, supported with measurements. The remainder of this paper is organized as follows. The signal model and measurements for UWB polarimetric analysis are described in Section II. Electromagnetic wave depolarization is characterized using an elliptical basis, and the statistics of the corresponding parameters of interest are estimated from the measurements in Section III. The dependence of the channel polarization properties on various parameters, such as the tap excess delay, delay spread, bandwidth, frequency, and small-scale space, is investigated in Section IV. Finally, conclusions are drawn in Section V.

II. SYSTEM MODEL AND MEASUREMENTS

A. Polarimetric Representation

Consider an elliptically polarized plane electromagnetic wave with Poynting vector **P** in the three-dimensional Cartesian space. Its electric field, **E**, can be decomposed using an
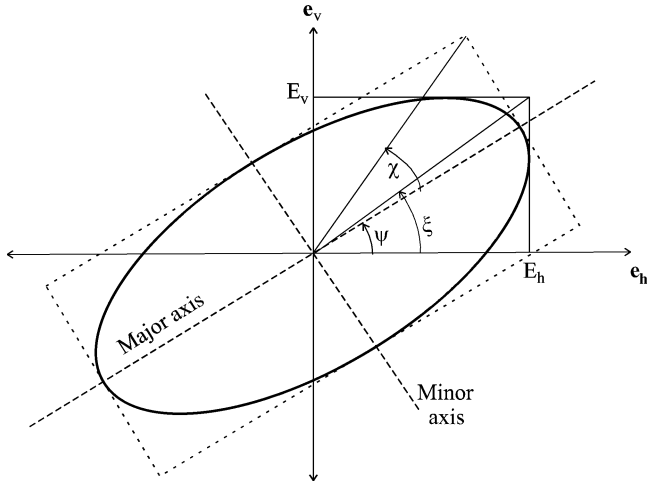
Fig. 1. Elliptical polarization basis for an electromagnetic wavefield.

Parameter	Symbol	Value
Start frequency	f_l	3.1 GHz
Stop frequency	f_h	10.6 GHz
Bandwidth	$W = f_h - f_l$	7.5 GHz
Number of frequency points	n_f	1601
Frequency resolution	$\Delta f = W/(n_f - 1)$	4.685 GHz
Time resolution	$\Delta t = 1/W$	0.133 ns
Transmit power	P_t	10 dBm
Low-noise amplifier gain	—	30 dB
Antenna type	—	Discone
Antenna height above ground	—	1.5 m

orthonormal basis with horizontal and vertical components perpendicular to $\mathbf{P}$, i.e.,

$$\begin{aligned}
\mathbf{E} &= E_v \hat{\mathbf{e}}_v + E_h \hat{\mathbf{e}}_h \\
&= |E_v| \exp\{j(-kz + \delta_v)\} \hat{\mathbf{e}}_v \\
&\quad + |E_h| \exp\{j(-kz + \delta_h)\} \hat{\mathbf{e}}_h
\end{aligned} \quad (1)$$

where $k = 2\pi f/c$ is the wavenumber, f is the frequency, $c = 3 \times 10^8$ m/s is the speed of light, and z corresponds to the direction of propagation. The horizontal and vertical orientations are represented by the unit vectors $\hat{\mathbf{e}}_v$ and $\hat{\mathbf{e}}_h$ respectively, while E_v and E_h are the complex amplitudes, and δ_v and δ_h the phase angles of the corresponding electric field components. The trace of the tip of the travelling wave defines an ellipse on a normal plane, as shown in Fig. 1. The ellipse reduces to a line (linear polarization) or circle (circular polarization) under special conditions [24]. This wave representation can be used to construct the Jones matrix, or the polarimetric scattering matrix, $\mathbf{s} \in \mathcal{C}^{2 \times 2}$, that describes the channel polarization response in terms of the complex transmitted and received signals, given by [25]

$$\mathbf{s} = \begin{bmatrix} E_{vv} & E_{vh} \\ E_{hv} & E_{hh} \end{bmatrix} \quad (2)$$

where E_{vh} refers to the complex field associated with a vertically polarized transmission and horizontally polarized reception, etc. The elliptical polarization representation can be converted to the Stokes-Mueller formulation using simple trigonometric transformations. Under the Mueller formalism, the Stokes vector of the incident wave can be transformed into that of the scattered wave through the Mueller matrix representing the channel [26], [27], facilitating convenient analysis of channel effects on the propagating wavefield.

For a radiated electromagnetic wave, $\mathbf{E} \perp \mathbf{P}$ as a consequence of Maxwell's equations. The antenna polarization properties are thus intrinsically coupled to its far-field radiation pattern. Consider an antenna that is omnidirectional in azimuth but directional in elevation when vertically polarized, such as a

dipole. When rotated by $90°$, its electric field becomes horizontally polarized, while the radiation pattern becomes directional in azimuth and omnidirectional in elevation. In other words, a variation in the orientation of an antenna with dipole-like gain inevitably changes not just the polarization but also the radiation pattern. Mobile devices in broadcast applications commonly use dipole-like elements that may undergo changes in orientation during operation. It is in the backdrop of this practical consideration that we conduct the polarimetric analysis in this paper. The results, therefore, include the effects of joint antenna polarization and pattern rotation as experienced by a range of omnidirectional antennas.

B. Propagation Measurements

The analysis in this paper uses 3.1–10.6 GHz UWB channel data obtained with a vector network analyzer (VNA). Indoor measurements are conducted in small office environments, consisting of approximately 6 m $\times$ 6 m rooms with block walls, glass windows, wooden and metallic furniture, and objects of various sizes and materials. The VNA RF ports are connected to the transmitting and receiving antennas, and the complex transmission parameter, $S_{21}(f)$, is measured. Two identical linearly polarized, omnidirectional discone antennas are used [28]. For NLOS measurements, the direct path is blocked with a large absorbent block placed between the antennas. Frequency-selective attenuation and phase distortion are calibrated. The measurement parameters are listed in Table I.

The location of the transmitter is fixed while the receiver, mounted on a computer-controlled grid positioner, scans a horizontal area as described in [7]. A measurement grid of size 1 m^2 samples the space at points 3 cm apart. The distance between the transmitter and the grid center is 4.5 m. The channel is temporally stationary during the measurement [7]. This process is repeated for the various transmit-receive polarization combinations and the LOS/NLOS propagation scenarios. The measured complex channel transfer function (CTF) is represented by the general form $\mathbf{g}_{ab}$, where $a, b \in \{v, h\}$ denote the transmit and receive polarizations, respectively. The four polarization combinations (vv, vh, hv, and hh) are measured sequentially so that there is only one antenna at each end at a time. The channel polarization state is then reconstructed from these single-polar antenna measurements using the linear component method [7], [29]. An ensemble, $\mathcal{R}$, of n_r measured channel realizations is

thus collected corresponding to each transmit-receive polarization combination.

C. Channel Data Processing

The rth polarized complex CTF, with transmit polarization a and receive polarization b, can be represented by

$$H_{ab}(r, f) = \sum_{n=1}^{n_f} A_{ab}(r, n) e^{j\theta_{ab}(r,n)} \delta(f - n\Delta f) \quad (3)$$

where A_{ab} and θ_{ab} denote the magnitude and phase response of the channel at the nth frequency point, measured by the VNA. The channel impulse response (CIR) is obtained as the inverse discrete Fourier transform of the CTF, and is given by

$$h_{ab}(r, \tau) = \sum_{n=1}^{n_\tau} \alpha_{ab}(r, n) e^{j\phi_{ab}(r,n)} \delta(\tau - n\Delta\tau) \quad (4)$$

where $\alpha_{ab}(r, n)$ and $\phi_{ab}(r, n)$ denote the amplitude and phase, respectively, at the nth time-bin, τ is the time-delay with reference to the first arrival, and n_τ is the number of delay bins in the CIR. We set the CIR power threshold to 20 dB below its peak in order to remove the noise and residual multipath, and designate the local maxima in the resulting CIR as the resolved multipath components (MPCs). Then, in terms of the MPCs, the tapped delay line representation of the CIR becomes

$$h_{ab}(r, \tau) = \sum_{l=1}^{L_{ab}(r)} \alpha_{ab}(r, l) e^{j\phi_{ab}(r,l)} \delta\left(\tau - \tau_{ab}(r, l)\right) \quad (5)$$

where $1 \le l \le L_{ab}(r)$ is the MPC index, α_{ab}, ϕ_{ab} and τ_{ab} denote the amplitude, phase and time delay of the lth MPC, and $L_{ab}(r)$ is the number of MPCs. The power delay profile (PDP), averaged over a local spatial region, shows the general trends of multipath clustering and impulse response decay with excess delay [30]. It is obtained from the CIR in (4) as

$$P_{ab}(\tau) = \mathcal{E}_{\mathcal{R}}\left\{|h_{ab}(r, \tau)|^2\right\} \quad (6)$$

where $\mathcal{E}_{\mathcal{R}}(.)$ denotes expectation over $\mathcal{R}$ and $r \in \mathcal{R}$. In (6), the CIRs are power-normalized so that $\int_0^\infty |h_{ab}(r, \tau)|^2 d\tau = 1$.

Fig. 2 shows the average PDPs, $P_{vv}(\tau)$ and $P_{hh}(\tau)$, corresponding to the LOS vv and hh channels respectively. Each PDP is normalized to its peak energy level, i.e. $\sup_\tau\{P_{ab}(\tau)\} = 1$. Some of the early paths form a small number of clusters, after which an almost linear decay of power is observed. For our measurement data, this feature is especially distinct in the vv channel, in which there is a sharp decay in the signal level between the first and second clusters, similar to the situation described by the Saleh-Valenzuela model [30]. On the other hand, significantly less energy disparity is observed among the initial timebins in the hh channel. In either case, the signal drops below -25 dB after approximately 50 ns. The average PDP will vary depending on the propagation environment. In particular, dense
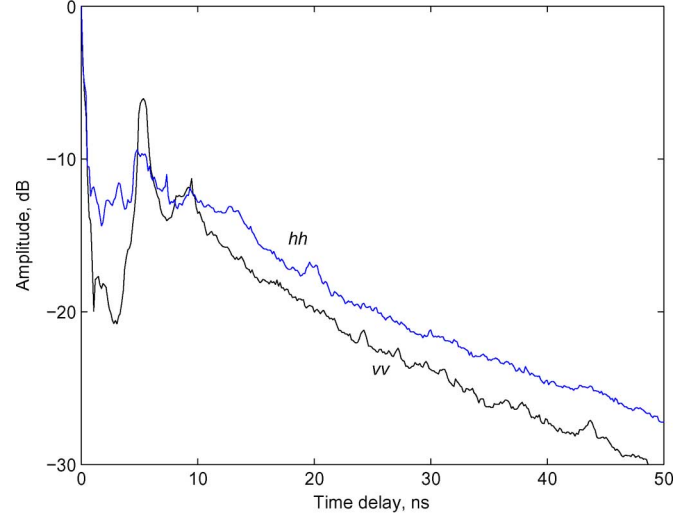

Fig. 2.   Locally averaged power delay profile (PDP) of the co-polar line-of-sight UWB channels.

multipath channels, such as industrial environments, will lead to PDPs with significantly slower decay rates.

III. CHANNEL POLARIZATION STATISTICS

We now analyze the polarization statistics of the UWB channel with bandwidth $W = 7.5$ GHz and center frequency $f_c = 6.85$ GHz. For the rth channel realization, the *composite* (i.e., all-polar) CIR magnitude for transmit polarization a is evaluated from the co- and cross-polarized CIRs as

$$|h_a(r, \tau)| = \sqrt{|h_{aa}(r, \tau)|^2 + |h_{ab}(r, \tau)|^2} \quad (7)$$

where the time-delay variable τ is now defined according to the first arrival above the threshold in the composite CIR, and $a \ne b$. The $L_a(r)$ MPCs of $h_a(r, \tau)$ are detected at time-bins $\tau_a(r, l)$, $l = \{1, \ldots, L_a(r)\}$. The corresponding set of $L_a(r)$ single-polar complex tap amplitudes, $h_{aa}(r, \tau_a)$ and $h_{ab}(r, \tau_a)$ are evaluated and stored in row vectors $\mathbf{h}_{aa}(r)$ and $\mathbf{h}_{ab}(r)$ respectively. We then define $\mathbf{H}_a(r) \in \mathcal{C}^{2 \times L_a(r)}$ whose elements are the co- and cross-polarized tap amplitudes, i.e., $\mathbf{H}_a(r) = [\mathbf{h}_{aa}^{\mathrm{T}}(r)\, \mathbf{h}_{ab}^{\mathrm{T}}(r)]^{\mathrm{T}}$. Finally, the tap amplitudes from the entire ensemble, $\mathcal{R}$, are collated into $\mathbf{H}_a^{\mathcal{R}} \in \mathcal{C}^{2 \times L_a^{\mathcal{R}}}$, where $L_a^{\mathcal{R}} = \sum_{r=1}^{n_r} L_a(r)$ and $\mathbf{H}_a^{\mathcal{R}} = [\mathbf{H}_a(r)]_{r=1}^{n_r}$. Thus each MPC amplitude in the measurement ensemble is treated as a single realization of a complex random variable. Since $\mathbf{H}_a^{\mathcal{R}}$ is a random matrix with a large ensemble, its elements and the related quantities can be modelled with continuous random variates. Their probability distributions and other statistics are estimated here using maximum likelihood parameter estimation.

The phase difference between the corresponding co- and cross-polarized MPCs is evaluated from $\mathbf{H}_a(r)$ as $\delta_a(r) = \arg\{\mathbf{h}_{aa}(r)\} - \arg\{\mathbf{h}_{ab}(r)\}$, where $-\pi \le \delta_a(r) \le \pi$. As $\phi_{aa}, \phi_{ab} \sim \mathcal{U}(-\pi, \pi)$, we expect $\delta_a(r)$ to also follow the uniform distribution, which is indeed confirmed from the data when the PDF of $\delta_a(r)$, $r \in \mathcal{R}$, is estimated. Next, we analyze the relative amplitudes of the co- and cross-polar components,
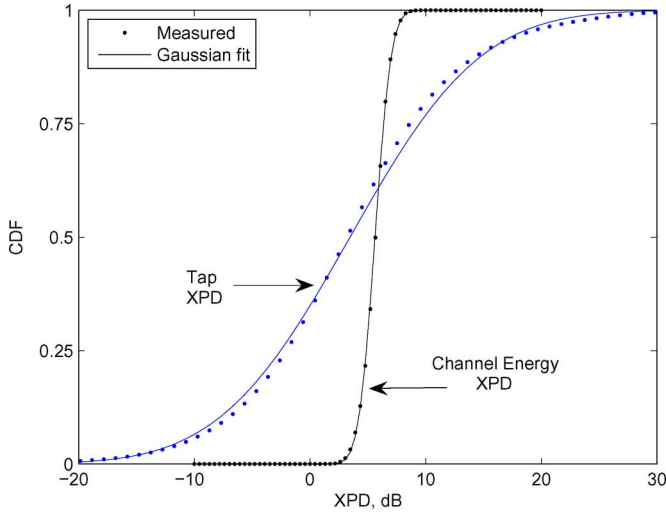
Fig. 3. Estimated and best-fit CDF of XPD with vertically polarized transmission in an LOS environment.

Fig. 4. Estimated and best-fit PDF of ellipticity angle of a multipath component in an LOS environment.

TABLE II
BEST-FIT GAUSSIAN DISTRIBUTION PARAMETER ESTIMATES FOR UWB
CROSS-POLAR DISCRIMINATION (XPD) IN DECIBEL SCALE

| Propagation | Transmit | Tap XPD (X_a) | | Energy XPD ($\mathcal{X}_a$) | |
Scenario	Polarization	Mean	Std.	Mean	Std.
LOS	v	4.0	8.9	5.8	1.1
LOS	h	5.6	8.4	5.6	0.9
NLOS	v	3.5	8.7	4.7	1.3
NLOS	h	4.3	8.4	3.5	1.1

which provide a measure of the channel's polarization preservation and coupling across orthogonal polarizations. The XPD is defined as the isolation between the received co-polar and cross-polar **E**-field components. For transmit polarization a, the tap XPD can be evaluated, in decibel scale, as

$$X_a(r) = 20 \left(\log_{10} |\mathbf{h}_{aa}(r)| - \log_{10} |\mathbf{h}_{ab}(r)| \right). \tag{8}$$

Perfect polarization preservation is indicated by $X_a \to \infty$, perfect depolarization by $X_a = 0$ dB, while $X_a < 0$ dB implies large coupling to the orthogonal polarization.

The estimated CDF of the single tap XPD, X_v, is shown in Fig. 3. The mean XPD, $\mathcal{E}_\mathcal{R}\{X_v(r)\}$, is found to be 4 dB, with 9 dB standard deviation. Similar values are obtained in NLOS, as seen from Table II. The large spread of the tap XPD indicates that the cross-polar power of an MPC can on occasion be much higher than the co-polar power. In comparison, X_h has a higher mean (5.5 dB in LOS). The difference in the polarization leakage suggests that the link is non-reciprocal in terms of polarization. Also shown in Fig. 3 is a Gaussian fit for X_v, using the parameters listed in Table II that provide a reasonable approximation for the tap XPD data.

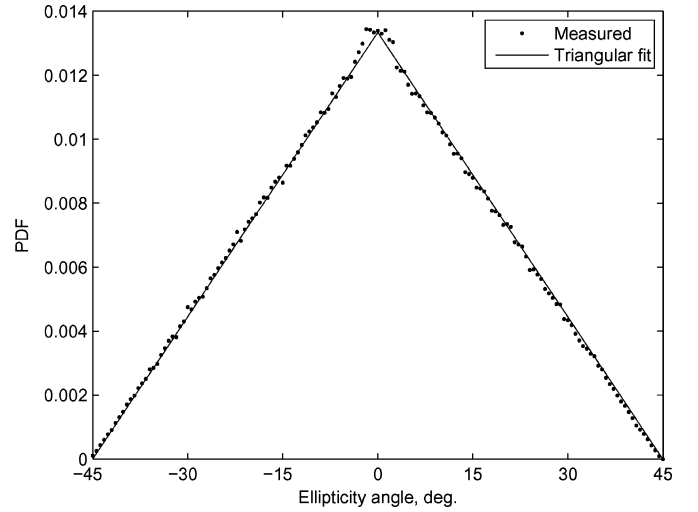Besides the tap amplitudes, also of interest here is the total channel energy, which represents the combined energy of all MPCs in the CIR as captured, for example, by an infinite-complexity maximal-ratio combining rake receiver. The channel energy can be evaluated as the squared l^2-norm of the channel tap vector. Mathematically, we can write

$$E_{ab}(r) = \sum_{l=1}^{L_{ab}(r)} |\alpha_{ab}(r,l)|^2 = |\mathbf{h}_{ab}(r)|^2. \tag{9}$$

The XPD of the UWB channel energy can then be evaluated from the co- and cross-polarized channel energy. For transmit polarization a, we evaluate the channel energy XPD in decibels (dB) as

$$\mathcal{X}_a(r) = 10 \left(\log_{10} E_{aa}(r) - \log_{10} E_{ab} \right). \tag{10}$$

The CDF of $\mathcal{X}_v$ is also shown in Fig. 3. It is evident that $\mathcal{X}_a$ enjoys substantially lower variance than X_a, $\forall a$. The mean $\mathcal{X}_a$ is 6 dB in LOS and 4 dB in NLOS, with 1 dB standard deviation. It can be shown that the XPD approaches its expected value asymptotically under large multipath diversity and with an appropriate receiver. Table II indicates the best-fit Gaussian distribution parameter estimates for $\mathcal{X}_a$.

The ellipticity angle of the incident **E**-field tap is given by

$$\chi_a(r) = \frac{1}{2} \sin^{-1} \left\{ \sin 2\xi_a(r) \sin \delta_a(r) \right\} \tag{11}$$

where $\xi_a(r) = \tan^{-1}\{\mathbf{h}_{ab}(r)/\mathbf{h}_{aa}(r)\}$ is the inclination angle of the co-polar electric field with the orthogonal axis, and $-\pi/4 \leq \chi_a(r) \leq \pi/4$. Fig. 4 shows the PDF of the tap χ_a, estimated over $\mathcal{R}$. As shown, a symmetric triangular distribution fit with $0°$ mean well approximates the measured χ_a. This result indicates that the polarization ellipse is usually significantly elongated, and the co-polarized component is generally much stronger than the cross-polarized component.

IV. IMPACT OF CHANNEL PARAMETERS

A. Temporal Variability

We now investigate the evolution of XPD with time-delay. The fine temporal resolution of the UWB channel facilitates this analysis for time intervals on the order of nanoseconds. The temporal evolution of polarization properties for ultrashort optical signals has been discussed in [31], but a similar study for radio channels is not available in the literature. For an indoor multipath UWB channel, this information will provide insight into the rate of decay of XPD for the received signal. Higher average XPD for specific MPCs can help improve the SNR when a vector (i.e., joint polarization and delay) selective-rake receiver is used [6]. The XPD decay rate assists in determining the integration time window for such a receiver.

The multipath excess delays, $\tau_a(r, l)$, corresponding to the composite channel $h_a(r, \tau)$ with transmit polarization a, populate the delay vector, $\mathbf{t}_a(r) = [\tau_a(r, l)]_{l=1}^{L_a(r)}$. The possible interdependence between $\mathbf{t}_a$ and X_a is analyzed in Fig. 5, which shows the variation of the measured $X_v(r)$ versus τ for $r \in \mathcal{R}$ in the LOS channel. We observe that X_v lies within the -30 dB to 40 dB range and has a large variance. Also, X_v is highest for the first 2 ns. The apparent decay in X_v with an increase in τ is confirmed by the negative slope of the best-fit regression line shown in the figure. Note that $X_a \to 0$ as $\tau \to \infty$ since the noise is completely depolarized, and so the regression is valid only for $0 \le \tau \le n_\tau \Delta\tau$. Significant dependence of XPD on τ for UWB channels is thus established. Our result contrasts with that reported for outdoor MIMO-HSDPA channels where no noticeable dependence of XPD on delay was observed [20]. We now quantify our observations by estimating the first order statistics of X_a across $\mathcal{R}$ for each delay tap. The mean and standard deviation of $X_v(r)$ thus obtained are shown in Fig. 6. The mean XPD is 25 dB for the direct path (corresponding to the observed dynamic range of the receiver, i.e., the VNA), but decays sharply with τ. Some clustering can be observed, as the mean $X_v(r)$ has its maxima at $\tau = \{0, 5\}$ ns but decays to 0 dB at $\tau = 4$ ns. A comparison with Fig. 2 reveals that the mean XPD mimics the behavior of the average PDP. The standard deviation of $X_v(r)$ is very low during the first 2 ns, after which it attains a constant value of 8 dB. Physically, the XPD has a large mean and small variance for paths that undergo little or no reflection since the propagation field does not undergo appreciable depolarization, as it does for the diffuse paths. In NLOS, the mean XPD is relatively more uniform across the delay axis due to the absence of the dominant direct path.

B. Effect of Channel Delay Spread

Given that the XPD depends on scattering, we now investigate its relation with the multipath delay spread of the channel. The rms delay spread, $\tau_a^\sigma(r)$, is a measure of the extent of multipath in the rth channel [30]. In earlier work, a negative correlation between XPD and τ_a^σ has been reported for narrowband channels [16], which agrees with intuition. The rms delay spread is evaluated using the composite CIR, $h_a(r, \tau)$ for $r \in R$, and plotted against the channel energy XPD, $\mathcal{X}_a(r)$, in Fig. 7. It is
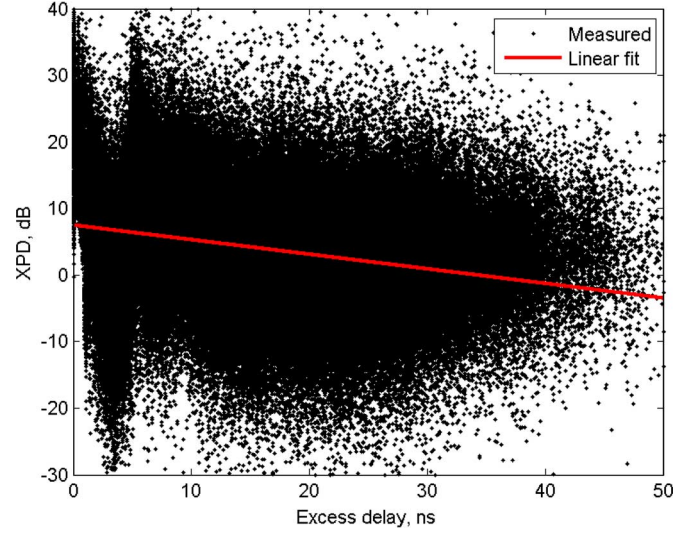

Fig. 5. Variation of XPD with the multipath excess delay spread with vertical transmit polarization in an LOS environment.
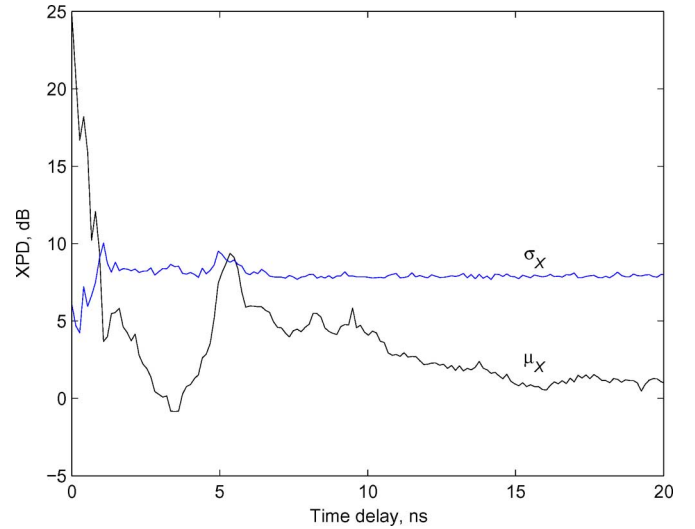

Fig. 6. Mean, μ_X, and standard deviation, σ_X, of XPD as a function of time delay with vertical transmit polarization in an LOS environment.

found that an increase in τ_a^σ leads to a decrease in $\mathcal{X}_a(r)$ in general. To quantify this dependence, we model $\mathcal{X}_a$ as a function of τ_a^σ with a linear regression, i.e.,

$$\log_{10} \bar{\mathcal{X}}_a(\tau_a^\sigma) = k_0 - k_\Delta \tau_a^\sigma + k_\sigma \qquad (12)$$

where k_0 is the intercept, k_Δ is the slope, and k_σ is a zero-mean Gaussian random variable signifying the variation about the mean XPD that has standard deviation σ dB. For the LOS channel with vertical transmission, we have $k_0 = 7$ dB, $k_\Delta = 0.5$ dB/ns, and $k_\sigma = 1$ dB. The other configurations exhibit only a minor difference in the values of these parameters. Now, earlier narrowband and wideband channel studies have shown the mean XPD to decrease with the transmitter-receiver separation, d [13]. In UWB channels, $\tau_a^\sigma \propto d$ [32], and it follows from
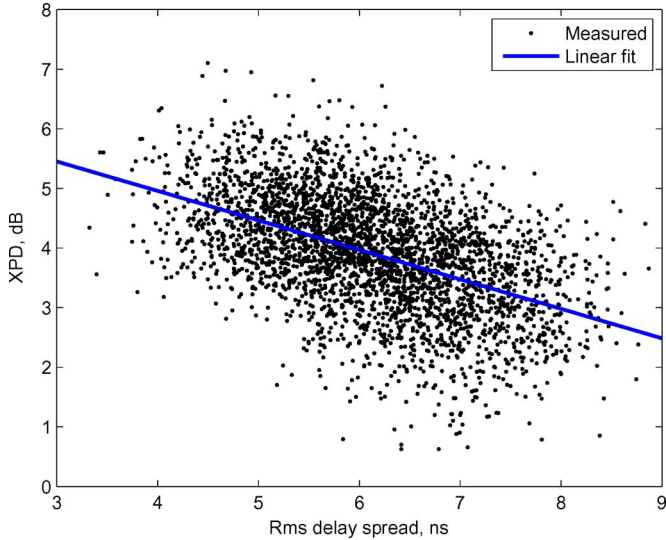
Fig. 7. Variation of XPD with the rms delay spread with a vertically polarized transmission in an LOS environment.

Fig. 8. Statistics of XPD as a function of frequency with the specified transmit polarization in an LOS environment.

the above discussion that $\mathcal{X}_a \propto d^{-1}$, extending previous results on distance-dependent XPD decay to UWB.

C. Variation With Center Frequency

The reflection coefficient of a scatterer determines the degree of depolarization of a polarized incident wave [24]. The reflection coefficient is in turn a function of frequency [33], and therefore spectrally nonuniform depolarization is expected in the UWB channel. This effect has been studied for optical communications in [34], [35], but not for frequency-selective radio channels. We now investigate this behavior, for which we evaluate the frequency-dependent XPD as

$$\mathcal{X}_a(r, f) = \left| \frac{H_{aa}(r, f)}{H_{ab}(r, f)} \right|^2. \qquad (13)$$

The first order statistics of $\mathcal{X}_a(r, f)$ are estimated over $r \in \mathcal{R}$. Fig. 8 shows the variation of the mean and standard deviation of $\mathcal{X}_a$, $a = \{v, h\}$, with frequency. We find that the XPD standard deviation is about 8 dB $\forall f$. Its mean, however, varies considerably over the band but without any discernible trend; for the LOS measurement, it is 6.5 dB at 4 GHz and 2.5 dB at 6.5 GHz. The main result from this analysis is the evidence of spectral variability of mean $\mathcal{X}_a(f)$, but its exact trends will depend on the propagation environment. The observation of greater polarization rotation at some of the subbands or subcarriers suggests that higher polarization diversity gain may be achieved at those frequencies. This spectral nonuniformity is in agreement with the variation of UWB small-scale channel statistics, such as delay spread, with the center frequency [36].

D. Dependence on Bandwidth

To characterize the XPD differences between narrowband, wideband and UWB channels, we now study its statistical variation with the channel bandwidth, $0 \leq W_b \leq W$. For the rth
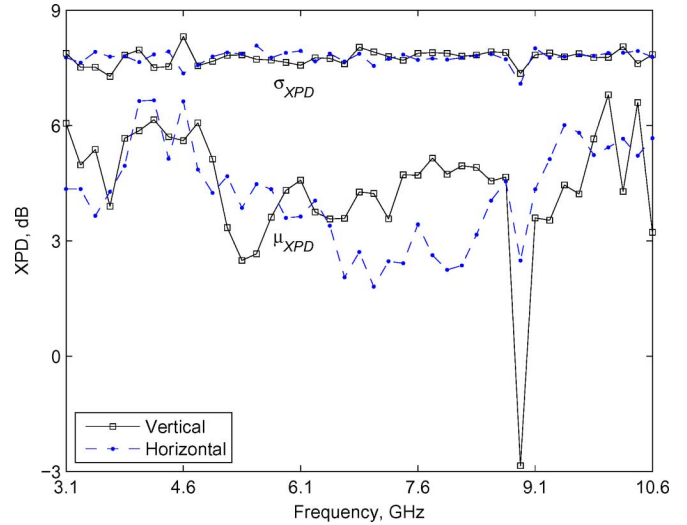
CTF, we calculate the energy XPD, $\mathcal{X}_a$, in terms of the co- and cross-polarized wideband channel energies, i.e.,

$$\mathcal{X}_a(r, W_b) = \frac{\int_{f_a}^{f_b} |H_{aa}(r, f)|^2 \, \mathrm{d}f}{\int_{f_a}^{f_b} |H_{ab}(r, f)|^2 \, \mathrm{d}f} \qquad (14)$$

where $f_a = f_c - W_b/2$ and $f_b = f_c + W_b/2$. The center frequency, f_c, is kept constant at 6.85 GHz for fair comparison. The mean and standard deviation of $\mathcal{X}_a(r, W_b)$, $r \in R$, are calculated, and are shown in Fig. 9. For both transmit polarizations, the standard deviation of narrowband $\mathcal{X}_a$ is 8 dB, decreasing exponentially with W_b to reach 1 dB at 1 GHz and 0.6 dB at 7.5 GHz. On the other hand, the mean $\mathcal{X}_a$ shows a minor variation with W_b. Considerable similarity is observed between the polarization statistics of the channels corresponding to the v and h transmit polarizations. We further characterize $\mathcal{X}_a$ by estimating its CDFs over $\mathcal{R}$ for various W_b, as shown in Fig. 10. The asymptotic convergence to the mean is closely related to the radio channel property of small-scale fade reduction with increasing W_b due to frequency diversity [37]. This effect can be quantified in terms of the coefficient of variation (CV) of $\mathcal{X}_a(r, W_b)$, which is the ratio of the standard deviation to the expectation and is given, as a percentage, by

$$\mathcal{X}_a^{CV}(W_b) = 100 \frac{\mathrm{std}_{\mathcal{R}} \{\mathcal{X}_a(r, W_b)\}}{\mathcal{E}_{\mathcal{R}} \{\mathcal{X}_a(r, W_b)\}}. \qquad (15)$$

We obtain $\mathcal{X}_a^{CV}(W_b) = 190\%$ and 16% in the narrowband and full-band UWB channels in LOS, respectively, demonstrating that the XPD randomness is reduced significantly with W_b.

E. Small-Scale Variability

The coherence distance of a full-band UWB channel is typically of the order of 5 cm [7]. The power variation across a larger distance is, however, minor due to the low fade range [37]. For this reason, we can expect the co- and cross-polarized
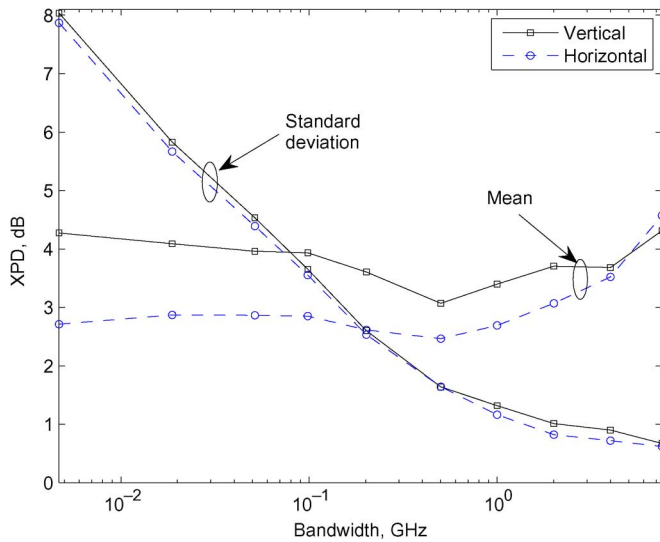
Fig. 9. Statistics of XPD as a function of bandwidth with the specified transmit polarization in an LOS environment.

Fig. 11. Variation of XPD with the spatial offset from the grid center with a vertically polarized transmission in an LOS environment.
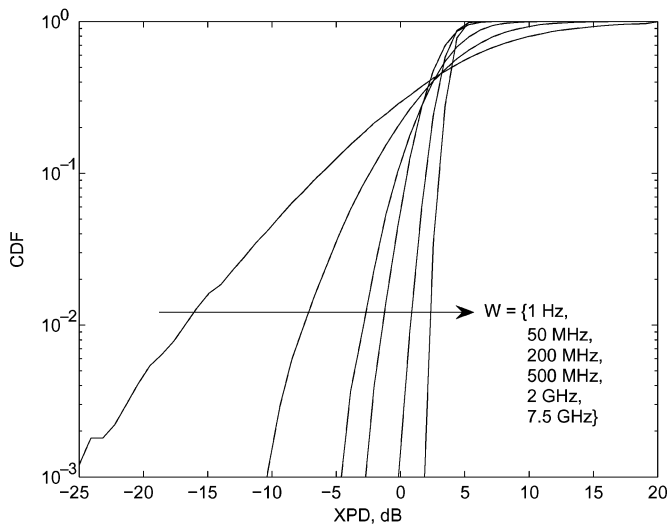

Fig. 10. Cumulative distribution function (CDF) of XPD as a function of bandwidth with vertically polarized transmission in an LOS environment.

channel energies to exhibit some small-scale spatial variation, which would then be reflected in a variation in the channel XPD, $\mathcal{X}_a$. Our small-scale analysis of $\mathcal{X}_a$, undertaken over a local region (1 m length) with a spatial resolution of 1 cm, confirms this prediction, with a set of representative results shown in Fig. 11. Along the cross-range direction, $\mathcal{X}_a$ fluctuates within 2 dB about its mean but there is no observable distance dependence. Similar ripples are observed along range, with a slow decrease in the mean $\mathcal{X}_a$ with distance that occurs due to increased scattering as discussed in Section IV-B.

V. CONCLUSION

In this paper, we have shown that the nonuniformity in the electrical properties of scattering objects over a large band results in frequency-selective XPD, setting the UWB channel apart from the narrowband channel from the polarization perspective. Certain subcarriers and subbands of the UWB channel
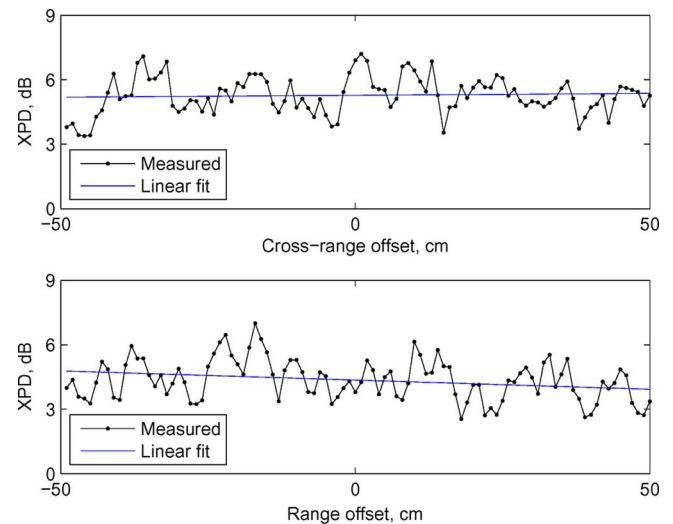
thus exhibit considerably larger XPD than the others. This variation is averaged out at large channel bandwidth, with the channel energy XPD distribution asymptotically converging to its mean. From our measurements, the mean XPD is 5 dB, independent of the channel bandwidth. Temporally, the mean $\mathrm{XPD} \geq 0$ dB at $\tau \leq 15$ ns, and is very large in the first 5 ns. With a vector selective-rake receiver, the integration of the initial MPCs is thus desirable. The relationship between signal depolarization and scattering has been established in terms of a linear model relating XPD to rms delay spread. The characterization in this paper extends the existing UWB channel models that do not contain any information on polarization. It also provides important analysis and design guidelines for single- and multiple-antenna UWB systems.

REFERENCES

[1] B. Allen, M. Dohler, E. E. Okon, W. Q. Malik, A. K. Brown, and D. J. Edwards, Eds., *Ultra-Wideband Antennas and Propagation for Communications, Radar and Imaging*. London, U.K.: Wiley, 2006.

[2] A. F. Molisch, "Ultrawideband propagation channels-theory, measurement, and modeling," *IEEE Trans. Veh. Technol.*, vol. 54, no. 5, pp. 1528–1545, Sep. 2005.

[3] R. G. Vaughan, "Polarization diversity in mobile communications," *IEEE Trans. Veh. Technol.*, vol. 39, no. 3, pp. 177–186, Aug. 1990.

[4] J. Jootar, J.-F. Diouris, and J. R. Zeidler, "Performance of polarization diversity in correlated Nakagami-m fading channels," *IEEE Trans. Veh. Technol.*, vol. 55, no. 1, pp. 128–136, Jan. 2006.

[5] L. Lukama, D. J. Edwards, and A. Wain, "Application of three-branch polarization diversity in the indoor environment," *Proc. Inst. Elect. Eng. Commun.*, vol. 150, no. 5, pp. 399–403, Oct. 2003.

[6] W. Q. Malik and D. J. Edwards, "UWB Impulse Radio with triple-polarization SIMO," in *Proc. IEEE Global Commun. Conf. (Globecom)*, Washington, DC, Nov. 2007, pp. 4124–4128.

[7] W. Q. Malik and D. J. Edwards, "Measured MIMO capacity and diversity gain with spatial and polar arrays in ultrawideband channels," *IEEE Trans. Commun.*, vol. 55, no. 12, pp. 2361–2370, Dec. 2007.

[8] M. R. Andrews, P. P. Mitra, and R. deCarvalho, "Tripling the capacity of wireless communications using electromagnetic polarization," *Nature*, vol. 409, pp. 316–318, Jan. 2001.

[9] M. Shafi, M. Zhang, A. L. Moustakas, P. J. Smith, A. F. Molisch, F. Tufvesson, and S. H. Simon, "Polarized MIMO channels in 3D: Models, measurements and mutual information," *IEEE J. Select. Areas Commun.*, vol. 24, no. 3, pp. 514–527, Mar. 2006.

[10] P. Kyritsi, D. C. Cox, R. A. Valenzuela, and P. W. Wolniansky, "Effect of antenna polarization on the capacity of a multiple element system in an indoor environment," *IEEE J. Select. Areas Commun.*, vol. 20, no. 6, pp. 1227–1239, Aug. 2002.

[11] K. Siwiak, "Ultra-wideband data communication system with diversity transmit and receive feature," U.S. Patent 20050152264, Jul. 2005.

[12] D. J. Edwards, T. Hao, W. Q. Malik, and C. J. Stevens, "A Planar Tripolar Antenna," U.K. British Patent, Pending.

[13] P. Soma, D. S. Baum, V. Erceg, R. Krishnamoorthy, and A. J. Paulraj, "Analysis and modeling of multiple-input multiple-ouput (MIMO) radio channel based on outdoor measurements conducted at 2.5 GHz for fixed BWA applications," in *Proc. IEEE Int. Conf. Commun. (ICC)*, New York, Apr. 2002, pp. 272–276.

[14] X. Zhao, S. Geng, L. Vuokko, J. Kivinen, and P. Vainikainen, "Polarization behaviours at 2, 5 and 60 GHz for indoor mobile communications," *Wireless Pers. Commun.*, vol. 27, no. 2, pp. 99–115, Nov. 2003.

[15] T. S. Rappaport and D. A. Hawbaker, "Wide-band microwave propagation parameters using circular and linear polarized antennas for indoor wireless channels," *IEEE Trans. Commun.*, vol. 40, no. 2, pp. 240–245, Feb. 1992.

[16] J. Toftgard and P. C. F. Eggers, "Experimental characterization of the polarization state dynamics of personal communication radio channels," in *Proc. IEEE Veh. Technol. Conf. (VTC)*, Secaucus, NJ, May 1993, pp. 65–69.

[17] S. Kozono, T. Tsuruhara, and M. Sakamoto, "Base station polarization diversity reception for mobile radio," *IEEE Trans. Veh. Technol.*, vol. VT-33, no. 4, pp. 301–306, Nov. 1984.

[18] J. J. A. Limpiainen and J. K. Laiho-Steffens, "The performance of polarization diversity schemes at a base station in small/micro cells at 1800 MHz," *IEEE Trans. Veh. Technol.*, vol. 47, no. 3, pp. 1087–1092, Aug. 1998.

[19] D. C. Cox, R. R. Murray, H. W. Arnold, A. W. Norris, and M. F. Wazowicz, "Cross-polarization coupling measured for 800 MHz radio transmission in and around houses and large buildings," *IEEE Trans. Antennas Propag.*, vol. AP-34, no. 1, pp. 83–87, Jan. 1986.

[20] A. F. Molisch, "On open questions of the MIMO channel model," in *3GPP-3GPP2 SCM-072*, Quebec City, Canada, 2002, Mitsubishi Electric Research Laboratories.

[21] D. Bicout and C. Brosseau, "Multiply scattered waves through a spatially random medium: Entropy production and depolarization," *J. Phys. I France*, vol. 2, no. 11, pp. 2047–2063, Nov. 1992.

[22] C. B. Dietrich, K. Dietze, and J. R. Nealy, "Spatial, polarization and pattern diversity for wireless handheld terminals," *IEEE Trans. Antennas Propag.*, vol. 49, no. 9, pp. 1271–1281, Sep. 2001.

[23] S. Chang and R. A. Scholtz, "Polarization measurements in a UWB multipath channel," in *Proc. IEEE Mil. Commun. Conf. (MILCOM)*, Monterey, CA, Oct. 2004, pp. 192–196.

[24] J. D. Kraus, *Electromagnetics*, 5th ed. New York: McGraw-Hill, 1999.

[25] F. T. Ulaby and C. Elachi, *Radar Polarimetry for Geoscience Applications*. Norwood, MA: Artech House, 1990.

[26] M. Born and E. Wolf, *Principles of Optics*. New York: Pergamon, 1989.

[27] S. R. Cloude, "Group theory and polarization algebra," *OPTIK*, vol. 75, no. 1, pp. 26–36, 1986.

[28] W. Q. Malik, D. J. Edwards, and C. J. Stevens, "Angular-spectral antenna effects in ultra-wideband communications links," *Proc. Inst. Elect. Eng. Commun.*, vol. 153, no. 1, pp. 99–106, Feb. 2006.

[29] J. D. Kraus, *Antennas*, 2nd ed. New York: McGraw-Hill, 1988.

[30] T. S. Rappaport, *Wireless Communications: Principles and Practice*, 2nd ed. Englewood Cliffs, NJ: Prentice Hall, 2001.

[31] W. J. Walecki, D. N. Fittinghoff, and A. L. Smirl, "Characterization of the polarization state of weak ultrashort coherent signals by dual-channel spectral interferometry," *Opt. Lett.*, vol. 22, no. 2, pp. 81–83, Jan. 1997.

[32] K. Siwiak, H. L. Bertoni, and S. M. Yano, "Relation between multipath and wave propagation attenuation," *Electron. Lett.*, vol. 39, no. 1, pp. 142–143, Jan. 2003.

[33] L. M. Frazier, "Radar surveillance through solid materials," in *Proc. SPIE*, Boston, MA, Feb. 1997, pp. 139–146.

[34] Y. Zhu, E. Simova, P. Berini, and C. P. Grover, "A comparison of wavelength dependent polarization dependent loss measurements in fiber gratings," *IEEE Trans. Instrum. Meas.*, vol. 49, no. 6, pp. 1231–1239, Dec. 2000.

[35] R. M. Craig, "Accurate spectral characterization of polarization-dependent loss," *J. Lightwave Technol.*, vol. 21, no. 2, pp. 432–437, Feb. 2003.

[36] W. Q. Malik, D. J. Edwards, and C. J. Stevens, "Frequency dependence of fading statistics for ultrawideband systems," *IEEE Trans. Wireless Commun.*, vol. 6, no. 3, pp. 800–804, Mar. 2007.

[37] W. Q. Malik, B. Allen, and D. J. Edwards, "Impact of bandwidth on small-scale fade depth," in *Proc. IEEE Global Commun. Conf. (Globecom)*, Washington, DC, Nov. 2007, pp. 3837–3841.

Wasim Q. Malik (M'05) received the B.E. degree from the National University of Sciences and Technology, Pakistan, in 2000 and the D.Phil. degree from the University of Oxford, Oxford, U.K., in 2005, both in electrical engineering.

From 2005 to 2007, he was a Research Fellow at the University of Oxford and a Junior Research Fellow in Science at Wolfson College, Oxford. Since 2007, he has been a Postdoctoral Fellow at the Massachusetts Institute of Technology, Cambridge. He is an editor of the book *Ultra-Wideband Antennas and Propagation for Communications, Radar and Imaging* (U.K.: Wiley, 2006), and was a Guest Editor of the *IET Microwaves Antennas and Propagation* Dec. 2007 Special Issue on Antenna Systems and Propagation for Future Wireless Communications. He has published in excess of 60 papers in refereed journals and conferences.

Dr. Malik received the ESU Lindemann Science Fellowship in 2007, the Best Paper Award in the ARMMS RF and Microwave Conf. (Steventon, U.K., April 2006), and the Association for Computing Machinery (ACM) Recognition of Service Award in 1997. He routinely serves on the organizing and technical program committees of various international conferences.